https://doi.org/10.1007/s41230-024-3158-y

Microstructure and mechanical properties of Co-28Cr-6Mo-0.22C investment castings by current solution treatment

Ze-yu Dan[1], Jun Liu[1], Jian-lei Zhang[1], Yan-hua Li[2], Yuan-xin Deng[2], **Yun-hu Zhang[1], and *Chang-jiang Song[1]

1. Center for Advanced Solidification Technology, School of Materials Science and Engineering, Shanghai University, Shanghai 200444, China

2. Wuxi CastPro Precision Co., Ltd., Wuxi 214105, Jiangsu, China

Abstract: This study examined the impact of current solution treatment on the microstructure and mechanical properties of the Co-28Cr-6Mo-0.22C alloy investment castings. The findings reveal that the current solution treatment significantly promotes the dissolution of carbides at a lower temperature. The optimal conditions for solution treatment are determined as a solution temperature of 1,125 °C and a holding time of 5.0 min. Under these parameters, the size and volume fraction of precipitated phases in the investment castings are measured as 6.2 μm and 1.1vol.%. The yield strength, ultimate tensile strength, and total elongation of the Co-28Cr-6Mo-0.22C investment castings are 535 MPa, 760 MPa, and 12.6%, respectively. These values exceed those obtained with the conventional solution treatment at 1,200 °C for 4.0 h. The findings suggest a phase transformation of $M_{23}C_6 \rightarrow \sigma+C$ following the current solution treatment at 1,125 °C for 5.0 min. In comparison, the traditional solution treatment at 1,200 °C for 4.0 h leads to the formation of $M_{23}C_6$ and M_6C carbides. It is noteworthy that the non-thermal effect of the current during the solution treatment modifies the free energy of both the matrix and precipitation phase. This modification lowers the phase transition temperature of the $M_{23}C_6 \rightarrow \sigma+C$ reaction, thereby facilitating the dissolution of carbides. As a result, the current solution treatment approach achieves carbide dissolution at a lower temperature and within a significantly shorter time when compared to the traditional solution treatment methods.

Keywords: CoCrMo alloy investment castings; current solution treatment; microstructure; mechanical property; carbide

CLC numbers: TG146.1+6 **Document code:** A

1 Introduction

With the rapid evolution of medical technology, there is a growing focus on advancing the research and application of medical biomaterials [1]. CoCrMo alloys, prized for their remarkable mechanical properties, corrosion resistance, wear resistance, and biocompatibility, have found extensive utilization in the fabrication of artificial implants, especially in hip and knee joints [2-5]. Produced by investment casting, CoCrMo components offer a cost-effective mean of creating intricate implant shapes [6]. However, in comparison to CoCrMo alloy components prepared via powder metallurgy and forging techniques, those produced by investment casting often exhibit diminished fatigue resistance and ductility [7-9]. This can be attributed to the uneven morphology, size, and distribution of carbides within the castings.

To address these challenges, heat treatment emerges as a conventional method for regulating the quantity and size of precipitation particles in alloy castings [10,11]. Solution treatment, a key component of this process, serves to dissolve carbides and regulate their distribution. It is noteworthy that a lower solution temperature fails to dissolve carbides [12], resulting in coarsening [13-15]. In addition, increasing the temperature leads to a reduction in carbide size, which can improve the plasticity and fatigue strength of the castings [16,17]. However, excessively high solution temperatures can lead to grain boundary melting and the formation of

***Chang-jiang Song**

Ph. D., Professor. His research interests mainly focus on solidification theory and microstructure control, and fabrication of super performance metastable engineering materials through solidification process control. He has supervised over 30 projects and published more than 130 papers in academic journals.

E-mail: riversong@shu.edu.cn; riversxiao@163.com

****Yun-hu Zhang**

E-mail: zhangyunhu.zyh@163.com

Received: 2023-11-30; Accepted: 2024-03-04

network precipitates, decreasing plasticity [18].

Furthermore, traditional solution treatments, even at elevated temperatures, are time-consuming. Consequently, the exploration of fast solution treatment methods is imperative for enhancing production efficiency. Recent literatures suggest that current heat treatment methods can swiftly regulate microstructure and improve mechanical properties at lower temperatures, owing to non-thermal effects such as electron wind [19,20] and electromigration [21,22]. The current, by reducing the diffusion activation energy of elements and augmenting diffusion rates, enhances heat treatment efficiency [23-25]. For instance, Wang et al. [26] demonstrated the current aging at 450 °C for 0.5 min achieved higher strength and plasticity in Fe-Mn-Al-C steel compared to traditional aging treatment at the same temperature for 3.0 h. The additional free energy introduced by current can lower the thermodynamic barrier, making it easier for precipitated phases to dissolve during solution treatment [27-30]. For instance, there was a significant decrease in the number of nano-precipitates in SA508-III steel after the current heat treatment at 430 °C for 3.0 min, a phenomenon that did not occur in traditional heat treatment at the same temperature and duration [31]. Zhou et al. [32] also observed a noticeable reduction in the size of carbides in high chromium iron castings after current heat treatment, transforming blocky carbides into smaller flakes or spheres. Despite the evident efficiency of current heat treatment in improving microstructure and properties in alloy components, its impact on CoCrMo alloy castings has been scarcely explored.

Therefore, this study aims to improve the solution treatment method for CoCrMo investment castings by incorporating the use of an electric current to enhance their mechanical properties. The microstructure and properties of the CoCrMo alloy castings by current solution treatment were compared to the ones by frequently-used traditional solution treatment. It also seeks to understand the mechanism behind current solution treatment for these castings.

2 Experimental procedures

2.1 Sample preparation and processing methods

Investment casting technology was employed to prepare Co-28Cr-6Mo-0.22C bar shaped castings with a diameter of 70 mm, which was subsequently sectioned into 80 mm×20 mm×3 mm plate-like samples using wire cutting. A rapid heat treatment furnace was utilized to perform current solution treatment on the CoCrMo samples, as depicted in Fig. 1. During the heat treatment process, both sides of the samples were connected to electrodes and heated at a rate of 8–9 °C·s^{-1} until reaching temperatures of 1,000 °C; 1,100 °C; 1,125 °C; and 1,150 °C, respectively. The samples were then held at each temperature for 10.0 min and rapidly cooled using an argon gas flow at a cooling rate of 35 °C·s^{-1}. Subsequent to mechanical properties testing, an optimal heat treatment temperature was identified, and various solution times were explored to investigate their impacts on the microstructure and properties of the casting. Optimized heat treatment parameters were then derived from this exploration. A comparative analysis was conducted among the samples treated with the identified optimal parameters, the as-cast samples, and the samples treated with traditional solution treatment. The latter involved holding the samples at 1,200 °C for 4.0 h and subsequently cooling with argon gas at a rate of about 1 °C·s^{-1}.

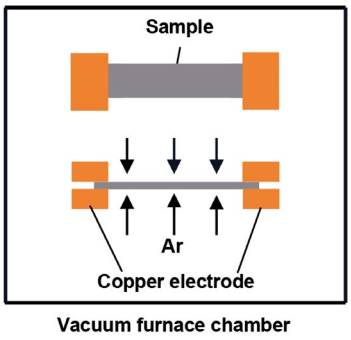

Fig. 1: Schematic diagram of current solution treatment equipment

2.2 Sample characterization and testing methods

The phase constitution analysis of samples was conducted using a 3kW D/Max-2200 rotating target X-ray diffractometer (XRD) with Cu Kα ray as the X-ray source, having a wavelength of 0.154056 nm. The detection parameters included a test voltage of 40 kV, a test current of 40 mA, a continuous scanning angle range from 40° to 60°, and a scanning rate of 2°·min^{-1}. To observe the microstructure, a Feiner Bench scanning electron microscope Pro XL was employed. In order to quantitatively analyze the carbides in castings, the volume fraction of the carbides in SEM images was measured using an ImageJ software. To ensure the accuracy of statistical data, more than 5 SEM images of each sample were selected for analysis. Electron probe microanalysis (EPMA) was performed using the EPMA-8050G equipment from Shimadzu Corporation in Japan.

SEM and EPMA samples were prepared by mechanical polishing followed by precision grinding until the surface achieved a bright, mirror-like appearance. Electrolytic corrosion was then induced using a 3wt.%–3.5wt.% nital solution [(3–3.5)wt.% nitric acid+(96.5–97)wt.% anhydrous ethanol] at 20 V for 10.0 s.

To assess room temperature tensile properties, the MTS Criterion 44 tensile testing machine was employed. The dimensions of the tensile specimen are depicted in Fig. 2. Its thickness is 1 mm. The stretching machine, with a maximum load of 10 kN, operated at a set stretching rate of 0.003 mm·s^{-1}.

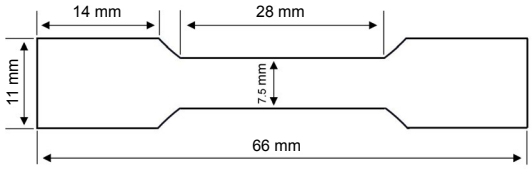

Fig. 2: Sizes of tensile specimen

An extensometer was horizontally clamped in the middle of the sample with a gauge distance of 25 mm.

3 Results

3.1 Effect of current solution treatment temperature on microstructure and properties

Figure 3 illustrates the XRD patterns of CoCrMo castings under various treatment conditions. The as-cast sample exhibits four peaks: (111)fcc, (200)fcc, $(10\bar{1}0)$hcp, and $(10\bar{1}1)$hcp at 2θ values of 43.75°, 50.75°, 41°, and 46.75°, respectively. Analysis indicates that the fcc phase corresponds to γ-Co, while the hcp phase corresponds to ε-Co [33]. The intensity of the $(10\bar{1}1)$hcp diffraction peak increases, and the intensity of the (200)fcc diffraction peak decreases after the current solution treatment at 1,000 °C for 10 min. The samples solutioned at 1,150 °C exhibit (111)fcc and $(10\bar{1}0)$hcp diffraction peaks. The intensity of the $(10\bar{1}0)$hcp diffraction peak continuously decreases as the temperature increases from 1,000 to 1,125 °C, and it nearly disappears when the solution temperature reaches 1,125 °C. Therefore, the current solution treatments exceeding 1,000 °C induce a phase transition from ε-Co to γ-Co in the castings. It is worth mentioning that the volume fraction of precipitated phases shown in Table 1 is relatively small, which is below the detection limit of the XRD equipment [34]. Consequently, the diffraction peak of precipitated phases could not be clearly observed.

Figure 4 presents backscattered electron (BSE) images of CoCrMo casting samples in the as-cast state and after current solution treatment at various temperatures for 10.0 min. Obviously, the precipitates in micron size are arranged nearly parallel in the matrix. The bright contrast of the precipitated phases indicates the presence of elements with high atomic numbers, such as Cr and Mo [35]. Under as-cast condition, the average size of precipitated phases is approximately 11 μm, the volume fraction is 7.1vol.% (Table 1). With increasing the temperature from 1,000 °C to 1,125 °C during current solution treatment, both the size and quantity of precipitated phases

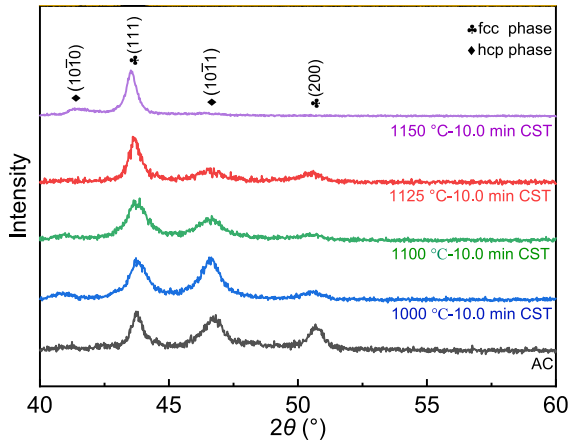

Fig. 3: XRD patterns of CoCrMo castings under different treatment conditions (AC means as-cast, CST means current solution treatment)

Table 1: Statistics of precipitated phases in CoCrMo castings under different treatment conditions

Sample	Average size of precipitates (μm)	Volume fraction (vol.%)
AC	11.0±1.2	7.1±0.4
1,000 °C/10.0 min CST	9.3±1.5	4.7±0.8
1,100 °C/10.0 min CST	8.6±1.7	4.3±0.4
1,125 °C/10.0 min CST	7.1±1.2	3.1±0.3
1,150 °C/10.0 min CST	13.2±1.4	7.8±0.8

decrease. At 1,125 °C, the average size and volume fraction of the precipitated phases reduce to 7.1 μm and 3.1vol.%, respectively. However, at 1,150 °C, the size and volume fraction of the precipitated phase increase again to 13.2 μm and 7.8vol.%, respectively.

The morphology of precipitated phase varies in the CoCrMo castings under different solution temperatures [Figs. 4(b, d, f, h, i)]. EDS analysis results in Table 2 identify the matrix (Area 1) in the as-cast sample as a Co-rich solid solution. The precipitated phases in Areas 2 and 3 are identified as $M_{23}C_6$ type carbides [36], with approximately 21.0at.% C and 41.0at.% Cr. The content of Mo is around 11.0at.%, while Co accounts for 23.0at.%. At 1,100 °C, two different precipitated phases appear [Fig. 5(f)]. The composition of dark phase (Area 4) is similar to $M_{23}C_6$, while the content of C, Co, and Cr elements of the white phase (Area 5) is different from the Co matrix and $M_{23}C_6$. According to the literatures [37-39], this white phase should be a σ phase. The σ phase is associated with the dissolution of $M_{23}C_6$ at high temperatures, where some carbides undergo $M_{23}C_6 \rightarrow C+\sigma$ reaction, and then, the decomposed C dissolves in the matrix [38]. The results of Figs. 4(g, h, i, j) and Table 2 indicate that the precipitated phase is mainly the σ phase when the temperature exceeds 1,100 °C; it has a higher brightness than $M_{23}C_6$ in the BSE images. When the temperature increases to 1,150 °C, both the size and volume fraction of σ phase increase.

Figure 5 shows the tensile curves of CoCrMo castings after solution treatment at different temperatures. The as-cast sample exhibits high ultimate tensile strength (UTS) and yield strength (YS) but a low ductility. Comparing to the as-cast sample, solution at 1,000 °C for 10.0 min results in increased UTS from 730 to 743 MPa and total elongation (TEL) from 6.1% to 6.8%, as shown in Table 3. But, as the solution temperature increases to 1,125 °C, the YS and UTS decrease to 515 MPa and 699 MPa, respectively, while the TEL increases to 10.6%. When the solution temperature exceeds 1,150 °C, the samples experience brittle fracture, as shown in Fig. 5. The YS of the samples after current solution treatment is generally lower than that of the as-cast sample, while the TEL is generally higher than that of the as-cast sample, except for 1,150 °C. The UTS of the samples is slightly higher at 1,000 °C, while others are lower than that of the as-cast sample.

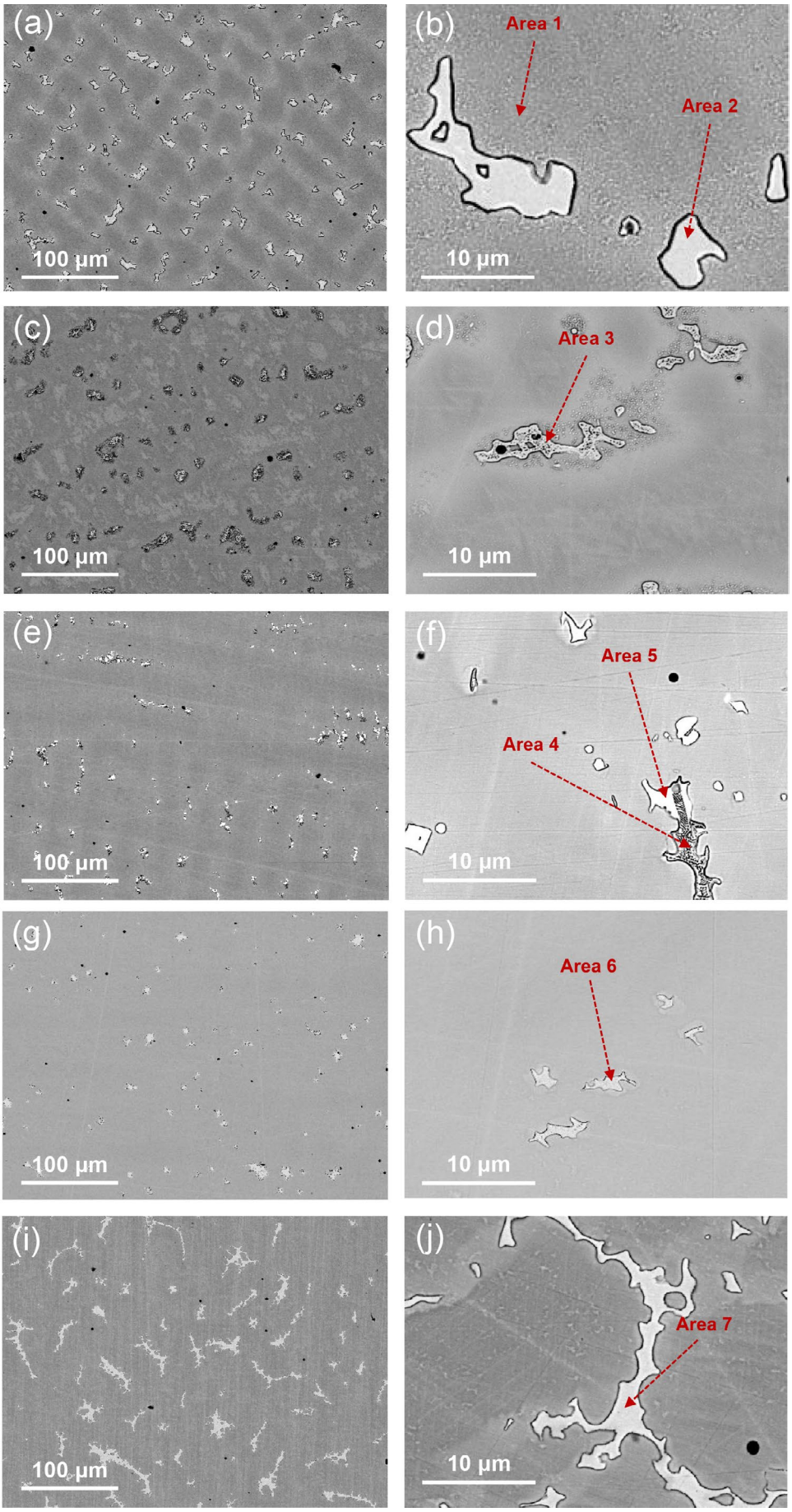

Fig. 4: SEM BSE images of CoCrMo castings before and after current solution treatment for 10.0 min: (a) and (b) as-cast; (c) and (d) 1,000 °C; (e) and (f) 1,100 °C; (g) and (h) 1,125 °C; (i) and (j) 1,150 °C

Table 2: EDS analysis of SEM images shown in Fig. 3 (at.%)

Area	Co	Cr	Mo	C	Si
1	61.3	31.3	4.1	1.2	2.1
2	23.7	40.4	11.7	21.5	2.7
3	22.5	41.5	10.9	22.2	2.9
4	22.7	42.0	12.0	20.5	2.8
5	43.3	33.5	10.0	10.8	2.4
6	45.2	32.0	10.4	9.7	2.7
7	43.3	32.8	10.3	11.1	2.5

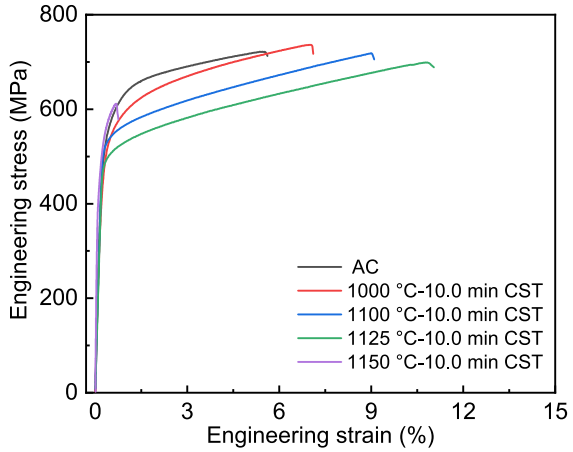

Fig. 5: Tensile curve of CoCrMo castings under different treatment conditions (AC is as-cast, CST is current solution treatment)

Table 3: Strength and elongation of CoCrMo castings under different treatment conditions

Sample	YS (MPa)	UTS (MPa)	TEL (%)
AC	562±5	730±10	6.1±0.9
1,000 °C/10.0 min CST	547±9	743±8	6.8±0.8
1,100 °C/10.0 min CST	539±6	716±6	9.1±1.0
1,125 °C/10.0 min CST	515±8	699±11	10.6±0.8
1,150 °C/10.0 min CST	551±7	618±8	1.8±0.2

3.2 Effect of current solution treatment time on microstructure and properties

As mentioned above, current solution treatment at 1,125 °C can significantly reduce the precipitated phases while enhancing ductility. Thus, an investigation was conducted to explore the impact of different solution times at 1,125 °C.

Figure 6 shows the XRD patterns of CoCrMo castings after current solution treatment at 1,125 °C for various durations (2.5, 5, and 10 min). After treated for 2.5 min, the XRD pattern shows four main peaks representing fcc and hcp phases. With increasing the treatment time, the intensity of (200)fcc and $(10\bar{1}1)$hcp peaks decreases and disappears at 10.0 min, leaving the (111)fcc and weaker $(10\bar{1}0)$hcp diffraction peaks. This indicates a phase transition from ε-Co to γ-Co with prolonged current solution treatment time at 1,125 °C.

Figure 7 shows the BSE images of CoCrMo casting after the current solution treatment at 1,125 °C for different times. The BSE microstructure images indicate the presence of σ phase, with the size and volume fraction showing a trend of decreasing at first and then increasing as the processing time extends. At 5.0 min, the microstructure exhibits the least σ phase, with an average size of 6.2 μm and the volume fraction of 1.1vol.%, as shown in Table 4.

Figure 8 shows the mechanical properties of the castings after current solution treatment at 1,125 °C for different times. The YS decreases continuously with increasing the treatment time, and it reduces to 515 MPa at 10.0 min, as shown in Table 5. The

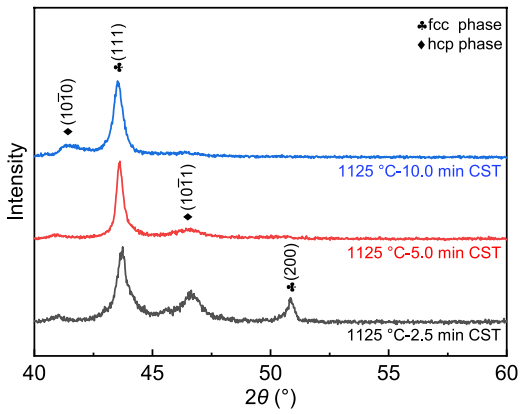

Fig. 6: XRD patterns of CoCrMo castings after current solution treatment (CST) at 1,125 °C for various durations

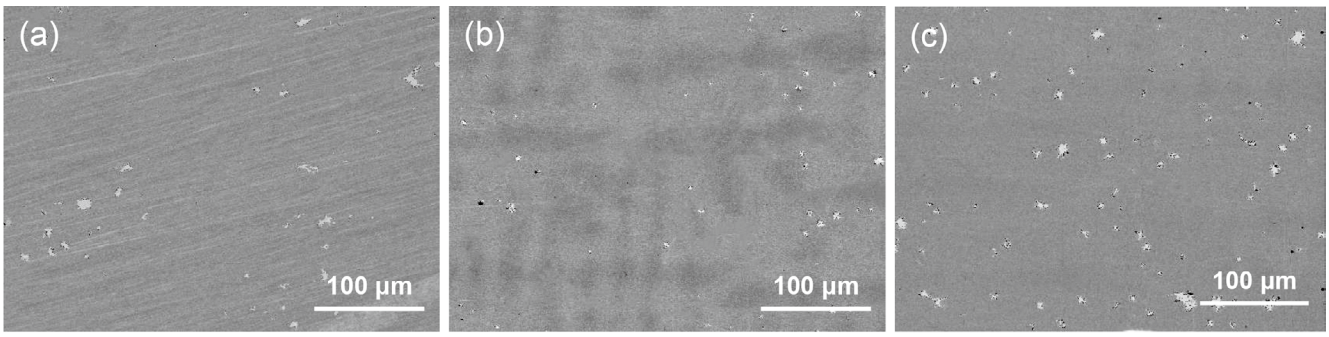

Fig. 7: BSE images of CoCrMo castings after current solution treatment at 1,125 °C: (a) 2.5 min; (b) 5.0 min; (c) 10.0 min

Table 4: Statistics of precipitated phases in CoCrMo castings after current solution treatment at 1,125 °C

Time	Average size of precipitates (μm)	Volume fraction (%)
2.5 min	7.3±0.8	2.6±0.4
5.0 min	6.2±0.9	1.1±0.2
10.0 min	7.1±1.2	3.1±0.3

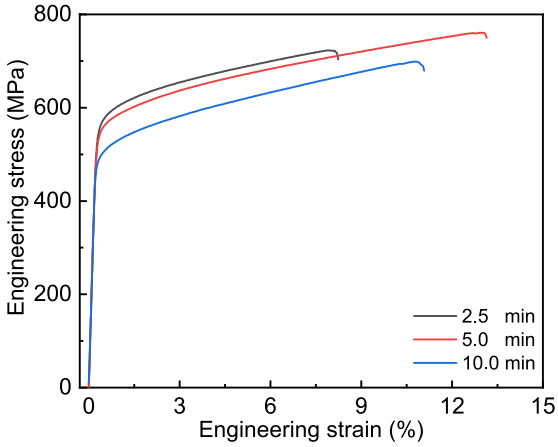

Fig. 8: Tensile curves of CoCrMo castings after current solution treatment at 1,125 °C for various durations

Table 5: Tensile properties of CoCrMo castings after current solution treatment at 1,125 °C

Time	YS (MPa)	UTS (MPa)	TEL (%)
2.5 min	550±10	723±9	8.2±0.6
5.0 min	535±6	760±8	12.8±0.3
10.0 min	515±8	699±11	10.6±0.8

CoCrMo casting achieves the best mechanical properties after current solution treatment at 1,125 °C for 5.0 min, with the UTS of 760 MPa and TEL of 12.8%.

3.3 Comparison between traditional solution treatment and current solution treatment

A sample after traditional treated at 1,200 °C for 4.0 h (which are optimal parameters for traditional solution treatment) and a sample after the current solution treated at 1,125 °C for 5 min were selected for comparative study. Figure 9 shows the corresponding XRD patterns of CoCrMo castings. The sample after the traditional solution treatment at 1,200 °C for 4.0 h still retains $(10\bar{1}1)$hcp and (200)fcc peaks, although their intensities are smaller than those in the as-cast sample. However, the intensity of the $(10\bar{1}1)$hcp diffraction peak in the sample treated by current solution is lower than that in the sample treated by traditional solution. This suggests that current solution treatment is more effective in promoting the transformation of the matrix from ε-hcp to γ-fcc.

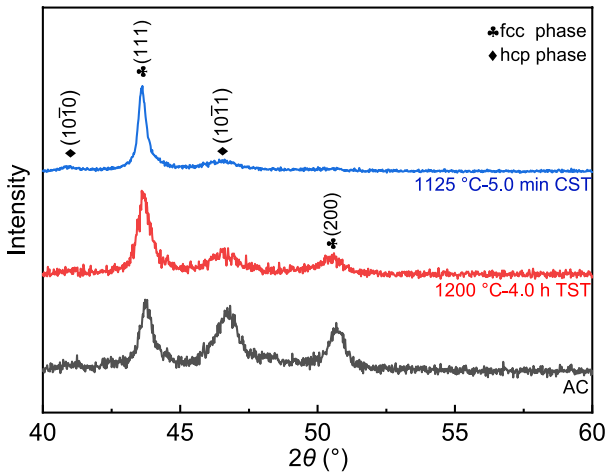

Fig. 9: XRD diagram of CoCrMo castings as-cast (AC) and after traditional solution treatment (TST), current solution treatment (CST)

EPMA-mapping was performed on CoCrMo casting samples after traditional solution treatment and current solution treatment to show the elemental distribution, as shown in Fig. 10. A cluster structure with different brightness presents in the sample after traditional solution treatment, as shown in Fig. 10(a). The Cr content in the gray area is significantly higher than that in the white area, while Co and Mo contents are lower in the gray area. This enrichment of Cr and Mo elements in the specific structure aligns with previous research [40]. The results of Fig. 4 and Table 2 indicate that the precipitated phase in Fig. 10(b) is σ phase. The contents of C and Cr elements in the gray area of Fig. 10(a) are higher than that of σ phase, while the content of Cr element in the white area is lower than that of σ phase. Thus, the precipitated phase in the sample treated by traditional solution is not σ phase. The precipitated phase in the grey area is identified as $M_{23}C_6$, and those in the white area are M_6C which obtained by decomposition of $M_{23}C_6$ during high-temperature solution, according to literatures [41, 42].

Figure 11 shows the BSE images of the microstructure after traditional solution treatment and current solution treatment, and the measured results of precipitated phases are shown in Table 6. After traditional solution treatment at 1,200 °C for 4.0 h, the size and volume fraction of carbides are 6.7 μm and 4.1vol.%, respectively. In contrast, the size and volume fraction of σ phase decrease to 6.2 μm and 1.1vol.% after the current solution treatment at 1,125 °C for 5.0 min. This indicates that current solution treatment is more efficient in reducing the precipitated phases, showing better solution ability compared to the traditional solution treatment.

Figure 12 and Table 7 show the tensile curves and mechanical properties of CoCrMo castings after traditional solution and current solution treatments. It can be seen that the casting treated by current solution has better mechanical properties than the casting treated by traditional solution. The YS, UTS, and TEL of the sample after current solution treatment at 1,125 °C for 5.0 min are 535 MPa, 760 MPa, and 12.8%, respectively, obviously higher than those after traditional solution treatment.

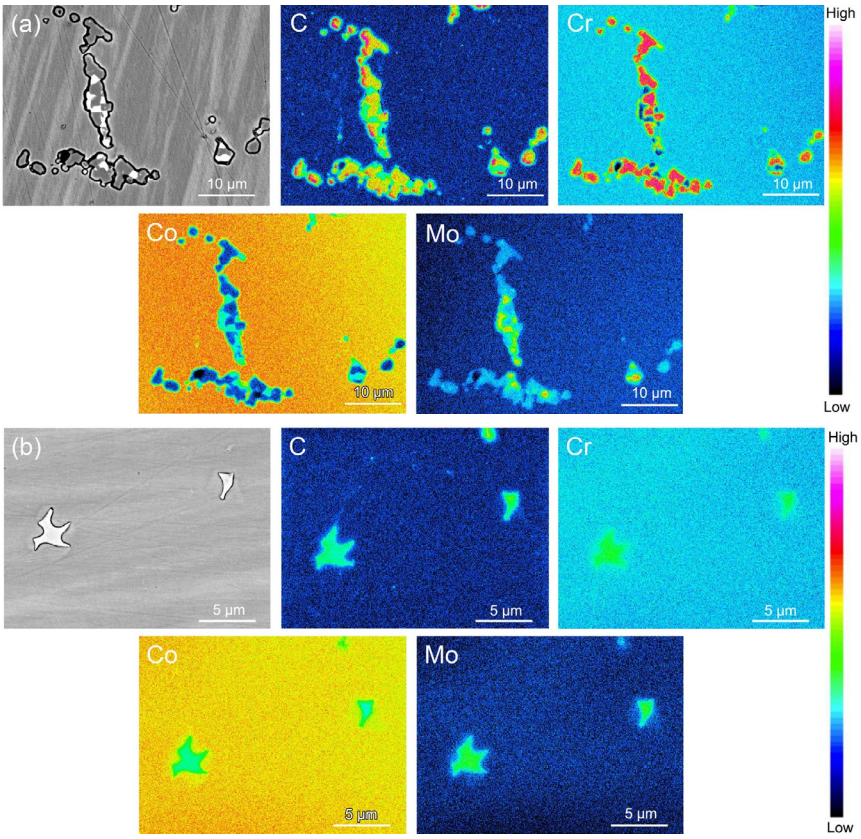

Fig. 10: EPMA-mapping diagram of CoCrMo castings after two different solution treatment methods: (a) traditional solution treatment; (b) current solution treatment

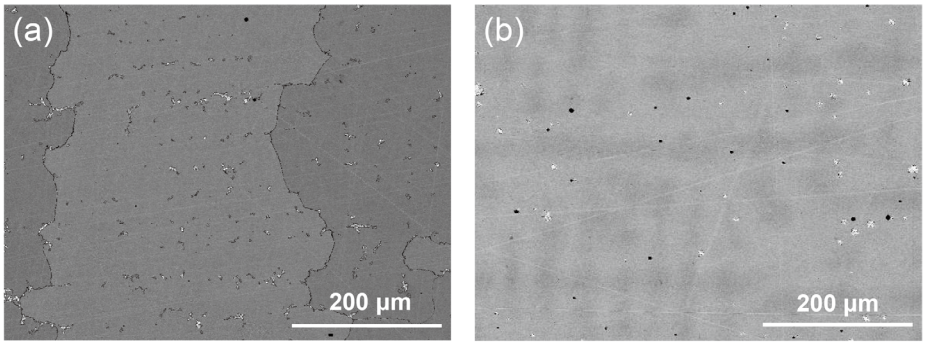

Fig. 11: BSE images of CoCrMo castings after two different methods: (a) 1,200 °C/4.0 h traditional solution treatment; (b) 1,125 °C/5.0 min current solution treatment

Table 6: Size and volume fraction of precipitated phases in CoCrMo castings under traditional solution treatment (TST) and current solution treatment (CST)

Sample	Average size of precipitates (μm)	Volume fraction (%)
1,200 °C-4.0 h TST	6.7±1.1	4.1±0.6
1,125 °C-5.0 min CST	6.2±0.9	1.1±0.2

4 Discussion

According to the phase diagram of CoCrMo alloys and previous studies, the as-cast CoCrMo casting is composed of a Co-rich matrix ε-phase with hcp structure and carbides [43]. However, as the XRD results shown in Fig. 3, the as-cast CoCrMo exhibits a dual-phase structure (γ-fcc+ε-hcp). This dual-phase structure

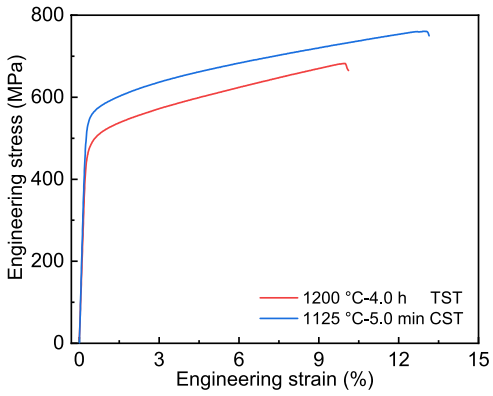

Fig. 12: Tensile curve of CoCrMo castings under traditional solution treatment (TST) and current solution treatment (CST)

Table 7: Mechanical properties statistics of CoCrMo castings under traditional solution treatment (TST) and current solution treatment (CST)

Sample	YS (MPa)	UTS (MPa)	TEL (%)
1,200 °C/4.0 h TST	494±8	680±3	9.9±0.7
1,125 °C/10.0 min CST	535±6	760±8	12.8±0.3

maybe result from the slow transformation from γ-fcc phase to ε-hcp phase during the cooling process in the investment casting.

During the current solution treatment, the carbides in the sample gradually dissolve into the matrix, as shown in Fig. 4. The fcc phase becomes dominant in CoCrMo casting after the current solution treatment at 1,125 °C for 10 min, as shown in Fig. 3 and Fig. 6. It indicates that the solution treatment at 1,125 °C not only results in the dissolution of carbides, but also stimulates the transformation of the matrix from ε-hcp to γ-fcc. Due to the fact that the slip system of γ-fcc is more than that of ε-hcp [35] and the reduction of carbides, the strength of the sample treated by current solution is reduced and the ductility is promoted compared to the as-cast sample.

However, as the solution treatment temperature and time are further increased, the volume fraction of high-temperature precipitated phases (i.e., σ phase, as shown in Fig. 4) increases, leading to a decrease in plasticity and tensile strength. According to Ishida's [44] research findings, it can be concluded that when the current solution treatment temperature is at 1,150 °C, there is a precipitation of the σ phase. The σ phase usually precipitates at the grain boundaries and forms a network structure, ultimately leading to a decrease in plasticity. Therefore, the mechanical properties of the sample are at their lowest level after current solution treatment at 1,150 °C for 10.0 min.

When current passes through a conductor, a great number of drift electrons form an electron stream that impacts metal atoms. Part of the energy of the electron stream is transferred to the atoms, increasing their energy and the overall temperature of the conductor. The temperature increase ΔT caused by Joule heat can be expressed as [45]:

$$\Delta T = \frac{j^2 R}{c_p \rho} \Delta t \tag{1}$$

where j is the current density, R is the conductor resistance, c_p is the specific heat capacity at constant voltage, ρ is the density of the conductor, and Δt is the current application time. In this experiment, after only 5.0 min of current solution treatment at 1,125 °C, the overall mechanical properties of samples are obviously improved compared to the samples after the optimal traditional solution treatment at 1,200 °C for 4 h. The YS, UTS, and TEL of the sample increase by 40 MPa, 80 MPa, and 3%, respectively, and the volume fraction of the precipitate decreases to 1.1vol.%. This indicates that current solution treatment is not only affected by Joule heating effect.

It is well known that the current in a conductor not only causes Joule heating effect, but also generates non-thermal effects (i.e. electromigration effect [47], electron wind force [48], and current magnetic effect [49], etc). During the current solution treatment process, the difference in conductivity between the matrix and the precipitated phases can result in the difference of their free energy change and affect the dissolution temperature of the second phase [49-51]. Moreover, current also accelerates solute atom diffusion, promoting carbide dissolution. The carbide dissolution during current solution treatment enhanced by coupling of thermal and electromigration effects can be described by [52-54]:

$$J_t = \frac{2\pi D_1}{\Omega \ln\left(\frac{R_0}{r_0}\right)} \cdot \left(1 + \frac{\delta_C}{c_0}\right) \tag{2}$$

$$J_a = \frac{N \cdot D_1 \cdot Z^* e \cdot \rho_0 \cdot j}{kT} \tag{3}$$

$$J = J_t + J_a = \frac{2\pi D_1}{\Omega \ln\left(\frac{R_0}{r_0}\right)} \cdot \left(1 + \frac{\delta_C}{c_0}\right) + \frac{N \cdot D_1 \cdot Z^* e \cdot \rho_0 \cdot j}{kT} \tag{4}$$

where the influence of current on atomic drift flux J is considered to be based on the coupling of thermal effect and electromigration effect. The thermal effect of current solution treatment, J_t, is the atomic flux generated by thermal activation effect during current solution treatment. The electromigration effect of current, J_a, is the atomic flux generated by the interaction between electrons and atoms. N is the atomic density, D_1 is the lattice diffusion coefficient, and c_0 is the average concentration of vacancies, δ_C is the supersaturated concentration of vacancies, r_0 and R_0 are the distance away from dislocations at vacancy concentrations of c_0 and $c_0 + \delta_C$, Z^* is the effective valence, and e is the charge, ρ_0 is the resistivity, and Ω is the atomic volume, k is the Boltzmann constant, and T is the absolute temperature. When the current treatment temperature increases, the current density j passing through the sample increases, resulting in an increase in the current drift flux J towards the atoms within the sample. The electromigration effect, combined with concentration gradients, promotes atom diffusion, leading to a rapid carbide solution. Therefore, the optimal dissolution effect is achieved at 1,125 °C, resulting in lower carbide size and volume fraction compared to traditional solution treatment.

The non-thermal effects of the current during solution treatment enhance the dissolution of carbides in CoCrMo castings. This allows for improvements in microstructures and mechanical properties at a lower temperature and in less time compared to traditional solution treatments. As a result, the current solution treatment emerges as a more effective method.

5 Conclusions

In this study, the microstructure and mechanical properties of Co-28Cr-6Mo-0.22C investment castings by current solution treatment were investigated. The following conclusions are drawn:

(1) The impact of current solution treatment temperature and time on CoCrMo precipitates reveals a non-linear trend. Initially, the size and volume fraction of precipitated phases decrease with increasing temperature and time, reaching their minimum at a solution temperature of 1,125 °C for 5.0 min, measuring 6.2 μm and 1.1vol.%, respectively. Simultaneously, mechanical properties achieve the optimal values: the YS, UTS and TEL are 535 MPa, 760 MPa, and 12.8%, respectively. When the temperature further increases, both the strength and ductility decrease due to precipitation of σ phase at grain boundaries.

(2) During the current solution at 1,125 °C, a transition from ε-hcp to γ-fcc occurs, the casting microstructure predominantly exhibits the γ-fcc phase. During current solution at 1,150 °C, the σ phase would precipitate, and the contents of C, Co, and Cr elements in the σ phase fall between the chemical compositions of the Co matrix and $M_{23}C_6$.

(3) Comparative analysis reveals a 3vol.% reduction in the volume of precipitated phases after current solution treatment at a relatively lower temperature and a shorter time, accompanied by a better mechanical property. This indicates that the current solution treatment has a higher efficiency to achieve carbide solution than the traditional methods, resulting in enhanced mechanical properties. This improvement in microstructure and performance is attributed to the non-thermal effects induced by the current.

Acknowledgments

This work was financially supported by the National Natural Science Foundation of China (Nos. 52271034, 51974183, and 51974184), Science and Technology Major Project of Yunnan Province (No. 202302AB080020), and Natural Science Foundation of Shanghai (No. 22ZR1425000).

Conflict of interest

The authors declare that they have no known competing financial interests or personal relationships that could have appeared to influence the work reported in this paper.

References

[1] Grosgogeat B, Vaicelyte A, Gauthier R, et al. Toxicological risks of the cobalt-chromium alloys in dentistry: A systematic Review. Materials, 2022, 15(17): 5801.

[2] Henriques B, Bagheri A, Gasik M, et al. Mechanical properties of hot pressed CoCrMo alloy compacts for biomedical applications. Materials & Design, 2015, 83: 829–834.

[3] Yamanaka K, Mori M, Kuramoto K, et al. Development of new Co-Cr-W-based biomedical alloys: Effects of microalloying and thermomechanical processing on microstructures and mechanical properties. Materials & Design, 2014, 55: 987–998.

[4] Junior W C D S, Souza C M P D, Bortoli F D S, et al. Obtaining the predicted number of cycles of femoral prosthesis manufactured with ASTM F138 and ASTM F75 aloys, applying the method of finite element. Journal of Physics: Conference Series, São Paulo, 2021, 1730(1): 012026.

[5] Vaicelyte A, Janssen C, Le Borgne M, et al. Cobalt-chromium dental alloys: Metal exposures, toxicological risks, CMR classification, and EU regulatory framework. Crystals, 2020, 10(12): 1151.

[6] Augustyn N J, Pełka S, Loch Z J. The effect of heat treatment on the microstructure and properties of the corrosion resistance of the prosthetic alloy Wironit ExtraHart (Co-Cr-Mo). Metallurgy and Foundry Engineering, 2018, 44(4): 181–193.

[7] Xu Q Y. Research on numerical modeling of investment casting process. Foundry, 2022, 71(7): 803–813. (In Chinese)

[8] Lee S H, Takahashi E, Nomura N, et al. Effect of heat treatment on microstructure and mechanical properties of Ni- and C-Free Co-Cr-Mo alloys for medical applications. Materials Transactions, 2005, 46(8): 1790–1793.

[9] Thomas J F, Alan K, Greg D, et al. The effect of melt temperature on the mechanical properties of cast ASTM F75 CoCrMo alloy as explained by nitrogen and oxygen content. Journal of Materials Research and Technology, 2020, 9(5): 9479–9486.

[10] ÖztÜrk K, ErtuĞrul O, Özcan M. Effects of various heat treatments on microstructure and mechanical properties of investment cast Co-Cr-Mo implants. Cumhuriyet Science Journal, 2021, 42(4): 965–976.

[11] Sing S L, Huang S, Yeong W Y. Effect of solution heat treatment on microstructure and mechanical properties of laser powder bed fusion produced cobalt-28chromium-6molybdenum. Materials Science and Engineering: A, 2020, 769: 138511.

[12] Clemow A, Daniell B. Solution treatment behavior of Co-Cr-Mo alloy. Journal of Biomedical Materials Research, 1979, 13(2): 265–279.

[13] Shtansky D V, Nakai K, Ohmori Y. Crystallography and interface boundary structure of pearlite with M7C3 carbide lamellae. Acta Materialia, 1999; 47: 1105–1115.

[14] de Andrés C G, Caruana G, Alvarez L. Control of $M_{23}C_6$ carbides in 0.45C-13Cr martensitic stainless steel by means of three representative heat treatment parameters. Materials Science and Engineering: A, 1998, 241(1–2): 211–215.

[15] García D A C, Alvarez L, López V, et al. Effect of heat treatment on microstructure and mechanical properties of Ti-containing low alloy martensitic wear-resistant steel. China Foundry, 2023, 20(4): 329–338.

[16] Giacchi J, Morando C, Foranro O, et al. Microstructural characterization of as-cast biocompatible Co-Cr-Mo alloys. Materials Characterization, 2011, 62(1): 53–61.

[17] Torkamani S, Morakabati M, Seifollahi M, et al. Evaluation the effect of carbon and solution treatment on the microstructure and mechanical properties of ASTM F75 cast cobalt base alloy. Founding Research Journal, 2022, 6(1): 22034.

[18] Mancha H, Escalante J, Mendoza G, et al. $M_{23}C_6$ carbide dissolution mechanisms during heat treatment of ASTM F-75 implant alloys. Metallurgical and Materials Transactions A, 2001, 32: 979–984.

[19] Savenko V V. Electroplastic deformation by twinningmetals. Acta Mechanica et Automatica, 2018, 12(4): 259–264.

[20] Zhao S, Zhang R, Chong Y, et al. Defect reconfiguration in a Ti-Al alloy via electroplasticity. Nature Materials, 2021, 20(4): 468–472.
[21] Xu H, Liu M, Wang Y P, et al. Refined microstructure and dispersed precipitates in a gradient rolled AZ91 alloy under pulsed current. Materialia, 2021, 20: 101245.
[22] Shao H, Shan D, Wang K, et al. Influence of DC heat treatments on microstructure, residual stress, and hardness of Ti-6Al-4V alloy. Metallography, Microstructure, and Analysis, 2019, 8: 378–385.
[23] Huang X, Yan L, Zhang X. Electromigration-enhanced atomic diffusion to improve coating interface bonding. Scripta Materialia, 2021, 202: 114017.
[24] Liu X, Zhang D, Wang H, et al. Regulating solute partitioning utilized to decorate grain boundary for improving corrosion resistance in a model Al-Cu-Mg alloy. Corrosion Science, 2021, 181: 109219.
[25] Xiao H, Jiang S, Shi C, et al. Study on the microstructure evolution and mechanical properties of an Al-Mg-Li alloy aged by electropulsing assisted ageing processing. Materials Science and Engineering: A, 2019, 756: 442–454.
[26] Wang Z G, Shen C L, Zhang J L, et al. An accelerated aging assisted by electric current in a Fe-Mn-Al-C low-density steel. China Foundry, 2022, 19(5): 395–402.
[27] Liu X, Lu W, Zhang X. Reconstructing the decomposed ferrite phase to achieve toughness regeneration in a duplex stainless steel. Acta Materialia, 2020, 183: 51–63.
[28] Qin S, Ba X, Zhang X. Accelerated cluster dissolution using electropulsing for ultrafast performance regeneration. Scripta Materialia, 2020, 178: 24–28.
[29] Huang X, Zhang X. Current-driving dissolution of nanoscale brittle precipitates produced by spinodal decomposition in FeCrAl alloys. Journal of Alloys and Compounds, 2019, 805: 26–32.
[30] He L Z, Wei M X, Ning Q B, et al. Effects of applying direct current on microstructures and properties of 7B04 aluminum alloy during solid solution and artificial ageing. Rare Metal Materials & Engineering, 2020, 49(6): 1957–1962.
[31] Qin S, Ba X, Zhang X. Accelerated cluster dissolution using electropulsing for ultrafast performance regeneration. Scripta Materialia, 2020, 178: 24–28.
[32] Zhou R F, Chen H, Wang T D, et al. Effect of electric current pulse on morphology of carbides in hypereutectic high chromium cast iron. Transactions of Materials and Heat Treatment, 2011, 32(7): 57–61.
[33] Kajima Y, Takaichi A, Kittikundecha N, et al. Effect of heat-treatment temperature on microstructures and mechanical properties of Co-Cr-Mo alloys fabricated by selective laser melting. Materials Science and Engineering: A, 2018, 726: 21–31.
[34] Da Silva D J, Contieri R, Cremasco A, et al. The effect of cooling rate on the microstructure and hardness of as-cast Co-28Cr-6Mo alloy used as biomedical knee implant. International Journal of Metalcasting, 2022, 16(4): 2187–2198.
[35] Wang R, Qin G, Zhang E. Effect of Cu on martensite transformation of CoCrMo alloy for biomedical application. Journal of Materials Science & Technology, 2020, 52: 127–135.
[36] Mineta S, Namba S, Yoneda T, et al. Carbide formation and dissolution in biomedical Co-Cr-Mo alloys with different carbon contents during solution treatment. Metallurgical and Materials Transactions: A, 2010, 41: 2129–2138.
[37] Alfirano, Mineta S, Namba S, et al. Precipitates in as-cast and heat-treated ASTM F75 Co-Cr-Mo-C alloys containing Si and/or Mn. Metallurgical & Materials Transactions A, 2011, 42(7): 1941–1949.
[38] Rosenthal R, Cardoso B, Bott I, et al. Phase characterization in as-cast F-75 Co-Cr-Mo-C alloy. Journal of Materials Science, 2010, 45: 4021–4028.
[39] Lee S H, Nomura N, Chiba A. Significant improvement in mechanical properties of biomedical Co-Cr-Mo alloys with combination of N addition and Cr-enrichment. Materials Transactions, 2008, 49(2): 260–264.
[40] Balagna C, Spriano S, Faga M. Characterization of Co-Cr-Mo alloys after a thermal treatment for high wear resistance. Materials Science and Engineering: C, 2012, 32(7): 1868–1877.
[41] Bettini E, Eriksson T, Boström M, et al. Influence of metal carbides on dissolution behavior of biomedical CoCrMo alloy: SEM, TEM and AFM studies. Electrochimica Acta, 2011, 56(25): 9413–9419.
[42] Giacchi J V, Fornaro O, Palacio H. Microstructural evolution during solution treatment of Co-Cr-Mo-C biocompatible alloys. Materials Characterization, 2012, 68: 49–57.
[43] Okamoto H. Co-Cr (cobalt-chromium). Journal of Phase Equilibria, 2003, 24(4): 377–378.
[44] Ishida K, Nishizawa T. The Co-Cr (cobalt-chromium) system. Bulletin of Alloy Phase Diagrams, 1990, 11(4): 357–370.
[45] Sprecher A F, Mannan S L, Conrad H. On the temperature rise associated with the electroplastic effect in titanium. Scripta Metallurgica, 1983, 17(6): 769–772.
[46] Pierce D G, Brusius P G. Electromigration: A review. Microelectronics Reliability, 1997, 37(7): 1053–1072.
[47] Magargee J, Morestin F, Cao J. Characterization of flow stress for commercially pure titanium subjected to electrically assisted deformation. Journal of Engineering Materials and Technology, 2013, 135(4): 041003–041010.
[48] Xu X F, Zhao Y G, Ma B D, et al. Electropulsing induced evolution of grain-boundary precipitates without loss of strength in the 7075 Al alloy. Materials Characterization, 2015, 105: 90–94.
[49] Lu W J, Zhang X F, Qin R S. Stability of precipitates under electropulsing in 316L stainless steel. Materials Science and Technology, 2015, 31(13): 1530–1535.
[50] Kuznetsov Y M, Dorokhin M V, Zdoroveyshchev A V, et al. Galvanomagnetic and thermomagnetic phenomena in thin metal CoPt films. Uspekhi Fizicheskikh Nauk, 2023, 193(3): 331–339.
[51] Jeong K, Jin S W, Kang S G, et al. Athermally enhanced recrystallization kinetics of ultra-low carbon steel via electric current treatment. Acta Materialia, 2022, 232: 117925.
[52] Jiang Y B, Tang G Y, Guan L, et al. Effect of electropulsing treatment on solid solution behavior of an aged Mg alloy AZ61 strip. Journal of Materials Research, 2008, 23(10): 2685–2691.
[53] Conrad H. Effect of electric current on solid-state phase transformations in metals. Materials Science and Engineering A, 2000, 287: 227–237.
[54] Blech I A. Electromigration in thin aluminum films on titanium nitride. Journal of Applied Physics, 1976, 47: 1203–1208.